Available online at www.sciencedirect.com
ScienceDirect
Journal of the European Ceramic Society 31 (2011) 883–892
www.elsevier.com/locate/jeurceramsoc

Zirconium nitride nano-particulate reinforced Alon composites: Fabrication, mechanical properties and toughening mechanisms

X.J. Zhao [a,b], D.L. Chen [a,*], H.Q. Ru [b], N. Zhang [c]

[a] Department of Mechanical and Industrial Engineering, Ryerson University, Toronto, Ontario M5B 2K3, Canada
[b] Department of Materials Science and Engineering, School of Materials and Metallurgy, Northeastern University, Shenyang, Liaoning 110004, China
[c] Key Laboratory of Advanced Materials Technology, Shenyang University, Shenyang, Liaoning 110044, China

Received 8 July 2010; received in revised form 4 November 2010; accepted 21 November 2010
Available online 14 December 2010

Abstract

Aluminium oxynitride (Alon) exhibits excellent stability, high rigidity and good thermal shock resistance, but it has relatively low strength and poor fracture toughness. The aim of this investigation was to develop a new type of zirconium nitride (ZrN) nano-particulate reinforced Alon composites via a change of ZrO_2 nano-particles during sintering. A reduction of porosity and grain size was observed in the composite. With increasing amount of ZrN nano-particles up to 2.7%, the relative density, hardness, Young's modulus, flexural strength, and fracture toughness all increased. When the ZrN nano-particles exceeded 2.7%, while the flexural strength and fracture toughness decreased slightly, the density, hardness and Young's modulus continued to increase. Different toughening mechanisms including crack bridging, crack branching and crack deflection were observed, thus effectively increasing the crack propagation resistance and leading to a considerable improvement in the flexural strength and fracture toughness of the composites.

Keywords: Alon; ZrN; Strength; Toughness; Toughening mechanism

1. Introduction

Spinel-type aluminium oxynitride, $Al_{23}O_{27}N_5$, (Alon) is a solid solution of Al_2O_3 and AlN.[1] Since Yamaguchi and Yanagida[2] first reported the Alon synthesis method by carbothermic reduction and nitridation of Al_2O_3, a lot of studies on the Alon ceramic material have been done.[3–5] Due to its excellent chemical and mechanical properties such as high rigidity, good thermal shock resistance and chemical stability, Alon has become a potential ceramic material for high-performance structural and advanced refractory applications.[6,7] In addition, it has been processed into a fully dense transparent material which showed promising mechanical and optical properties suitable for use in infrared and visible window applications.[8]

Zirconium nitride (ZrN) is becoming an attractive material because of its excellent chemical and physical properties such as high chemical and thermal stability with a melting point of 2980 °C, high hardness, abrasive resistance and good electrical conductivity.[9,10] It has a number of technological applications such as refractory material,[11] hard coating for cutting tools[12] and Josephson junction in electronics.[13]

Zirconia (ZrO_2) is also an attractive candidate for high-temperature applications because of its relatively high melting point (2715 °C) and excellent corrosion resistance. It is also an important ceramic for transformation toughening.[14–16] Pure ZrO_2 can be used as an additive to enhance the mechanical properties of other oxide refractories. It is particularly advantageous for improving abrasive resistance when ZrO_2 is added to high-fired magnesia and alumina.[17] The use of such a transformation toughening behaviour would result in strong yet tough ceramic matrix composites.[18] Furthermore, it is of interest to notice that ZrN phase can be generated when the added ZrO_2 reacted with Si_3N_4 at temperatures in excess of 1600 °C.[19] It is unknown if ZrN phase would occur when the ZrO_2 is added to Alon, and how the ZrN phase affects the mechanical properties of Alon.

Much attention has been drawn to the development of Alon and Alon matrix composites in order to improve the mechanical properties such as flexural strength and fracture toughness.[20–23] Khan et al.[24] studied the crystal structure, surface morphology, elemental distribution and microhardness of ZrAlON film. A

* Corresponding author. Tel.: +1 416 979 5000x6487; fax: +1 416 979 5265.
E-mail address: dchen@ryerson.ca (D.L. Chen).

0955-2219/$ – see front matter © 2010 Elsevier Ltd. All rights reserved.
doi:10.1016/j.jeurceramsoc.2010.11.014

Table 1
The composition of raw powders (in wt%) selected for fabricating the ZrN–Alon composites in the present study.

No.	Alon	ZrO_2
A	100	0
B	97	3
C	94	6
D	91	9

number of other reinforcements, e.g., Al_2O_3[20] and TiN[22] particles, have been added to Alon matrix as well. However, to the authors' knowledge, no report on adding ZrN or ZrO_2 to Alon ceramics has been seen in the open literature, although ZrO_2 has been added to hydroxyapatite to increase the bending strength for the load-bearing orthopedic applications.[25] The questions remain if the ZrN phase can be generated via ZrO_2 addition and to what extent the ZrN phase can improve the mechanical properties of Alon ceramics and what the toughening and strengthening mechanisms are. The aim of this work was, therefore, to develop a new type of ZrN–Alon composites, evaluate their microstructure and mechanical properties, and identify the underlying toughening and strengthening mechanisms.

2. Materials and methods

In the present study a two-step procedure was adopted. The Alon powder was first prepared, and then the pure ZrO_2 powder was introduced into the crushed Alon powder to fabricate ZrN–Alon composites.

2.1. Synthesis of Alon powders

The starting materials in weight percent were 81% α-Al_2O_3, 18% AlN and 1% Al powders. Al powder was added as a reduction agent to ensure that the atmosphere lay in the stable region of Alon when Al was in equilibrium with both nitrogen and oxygen.[4] The thoroughly mixed powders were attrition milled for 24 h using ethanol as a milling medium. The milled powders were dried at 80 °C, and then synthesized at 1750 °C in nitrogen atmosphere for 2 h using solid synthesis method by reacting aluminium oxide (Al_2O_3) with aluminium nitride (AlN).[1] The heating rate was 10 °C/min. After synthesis, the powders were then ball-milled for 24 h to break down agglomerates using ethanol as a liquid medium. The dried powders were crushed using mortar and sieved through a 180 μm mesh.

2.2. Preparation of Alon composites

The prepared Alon powders and nano-sized ZrO_2 powders with mass ratios given in Table 1 were intimately mixed by attrition milling using ethanol as a liquid medium for 24 h, then dried at 80 °C. The dry mixed ZrO_2–Alon powders were crushed using mortar and then sieved through a 180 μm mesh. The mixed powders as well as pure Alon powders were put in a graphite die and sintered at 1850 °C under a pressure of 25 MPa for 40 min in nitrogen atmosphere using a heating rate of 10 °C/min below 1400 °C and then 5 °C/min up to the selected sintering temperature. Finally the sintered Alon composites were furnace-cooled down to room temperature.

2.3. Evaluation of microstructure and mechanical properties

The density or porosity of sintered samples was measured using two methods. One was the Archimedes principle using distilled water where the relative density and porosity could be determined; the other was the quantitative image analysis using scanning electron microscope (SEM) micrographs where five SEM images were used for each material. The phase and crystallinity were analyzed via X-ray diffraction (XRD) using CuK_α radiation at 45 kV and 40 mA, with a step size of 0.05° and duration of 1 s in each step. Some slow scans with a step size of 0.02° and duration of 8 s in each step were also conducted to identify the presence of ZrO_2 and ZrN. The microstructure including the powder size was examined via SEM. The elemental concentration profile of the microstructure was determined using energy dispersive X-ray spectroscopy (EDS). The Vickers microhardness was determined on the polished surface using a computerized microhardness tester at a load of 4.9 N for a dwell time of 15 s in accordance with ASTM C1327. Eleven indentations were made on each sample and the average values were reported.

The three-point bending (TPB) samples, with a dimension of 25 mm × 2 mm × 2 mm, were prepared and polished to a surface finish using 1 μm diamond paste. The TPB tests were performed with 1 kN load cell and using a TPB stage with a span of 20 mm attached to a computerized Instron 8801 fatigue testing system. In the TPB tests the cross-head speed was set at a rate of 0.2 mm/min in accordance with ASTM C1161. The values for bending strength σ, and Young's modulus E were calculated according to the following equations[26,27]:

$$\sigma = \frac{3FL}{2bh^2}, \tag{1}$$

$$E = \frac{kL^3}{4bh^3}, \tag{2}$$

where F is the load at failure (N), L is the span (mm), b is the sample width (mm) and h is the thickness (mm), k is the slope (dF/dv) in the load-deflection curve. To evaluate the slope k more accurately, a load range from 5 N to the maximum load was used in all the TPB tests.

Fracture toughness was determined using a Vickers indentation technique.[28]

$$K_c = \chi\left(\frac{E}{H}\right)^{1/2}\left(\frac{F_1}{a^{3/2}}\right), \tag{3}$$

where F_1 is the applied load (N), E is the Young's modulus (GPa), H is the Vickers hardness (GPa), a is the radial crack length (m) measured from the center of indent and χ is an empirically determined "calibration" constant taken to be 0.016 ± 0.004.[29] The fracture surfaces of the sintered ZrN–Alon composites after the TPB tests were examined via SEM to iden-

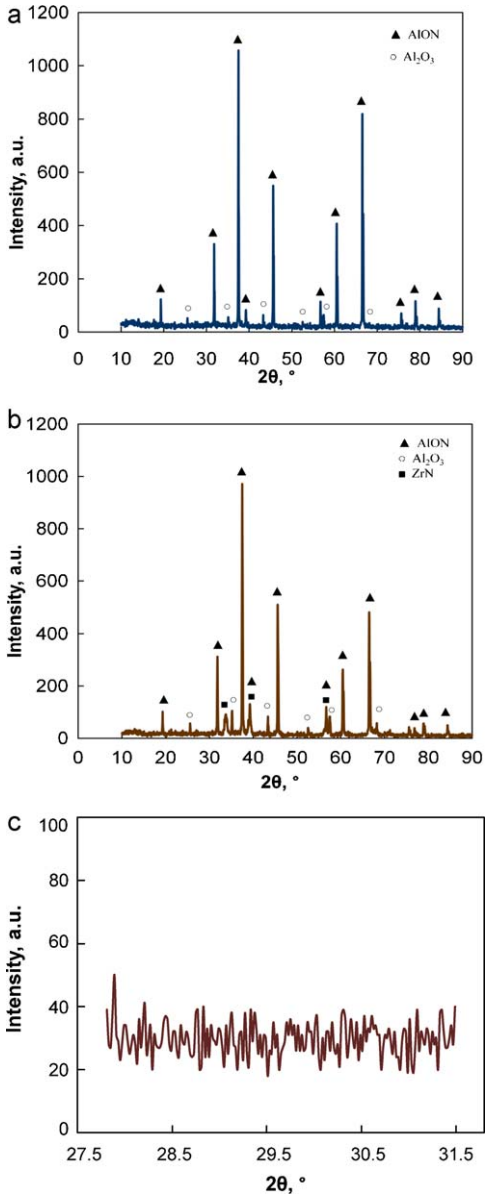

Fig. 1. XRD patterns of (a) pure Alon, (b and c) 2.7% ZrN–Alon composites sintered in a nitrogen atmosphere at 1850 °C, where (a) and (b) were obtained at a faster scan rate from 10° to 90° with a step size of 0.05° and duration of 1 s in each step, and (c) was acquired at a slower scan rate from 27.8° to 31.5° with a step size of 0.02° and duration of 8 s in each step.

tify the fracture mechanisms. To achieve a better resolution the SEM observations were done after the fracture surfaces were sputter-coated with a thin film of gold.

3. Results

3.1. X-ray diffraction analysis

Fig. 1 shows the XRD patterns of pure Alon and Alon composites with 6 wt% ZrO_2 addition. It is seen that the obtained pure Alon exhibited a typical XRD pattern of Alon without decomposition of other by-products (as seen in Fig. 1(a)). There was, however, a little bit Al_2O_3 phase left in the pure Alon or Alon composites. Other authors also observed that Al_2O_3 or AlN was present in the sintered samples, e.g., Qi et al.[30] reported that the synthesized Alon powders normally contained a little remaining Al_2O_3 or AlN. It is of interest to observe that after the hot press sintering at a high temperature of 1850 °C, neither m-ZrO_2 nor t-ZrO_2 was present, since no peaks at 28.2° and 30.3° corresponding to the highest intensity peaks of m-ZrO_2 and t-ZrO_2 appeared. Instead, the {1 1 1} peak of ZrN phase at about 33.7° was observed, together with other ZrN peaks appeared at about 39.1° and 56.5°, which corresponded to the second {2 0 0} and third {2 2 0} highest intensity peaks of ZrN, as shown in Fig. 1(b). The change of ZrO_2 to ZrN in Alon after the high temperature sintering is in agreement with the result reported in[19] where the added ZrO_2 became ZrN via reacting with Si_3N_4 at temperatures in excess of 1600 °C. To make sure that there was no ZrO_2 phase present in Alon composites after sintering in nitrogen atmosphere at 1850 °C, six samples were slowly scanned from 27.8° to 31.5° using XRD with one of the representative XRD spectra shown in Fig. 1(c). All of the XRD patterns showed the absence of ZrO_2 in the Alon composites. When 3 wt%, 6 wt% and 9 wt% ZrO_2 particles were added, and if the ZrO_2 was assumed to change into ZrN completely, the volume percent of ZrN phase in the ZrN–Alon composites was estimated to be about 1.4%, 2.7% and 4.1%, respectively, using density values of 5.68 g/cm^3, 7.09 g/cm^3, and 3.69 g/cm^3 for ZrO_2, ZrN, and Alon. It is seen from Fig. 1(b) that the Alon composites with 2.7% ZrN particles consisted mainly of Alon, ZrN and a small amount of Al_2O_3, and no other phases could be identified in the pattern.

3.2. Microstructure and density

Fig. 2 shows the SEM micrographs of the prepared Alon powders and nano-sized ZrO_2 powders. It is seen from Fig. 2(a) that the prepared Alon powders had a size of about 5 μm and a spinel-type structure as reported by Corbin.[1] Fig. 2(b) shows that all ZrO_2 particles were nano-sized (<100 nm), but there also appeared a conglomeration because it was rather difficult to disperse nanometer powders on the copper plate after ultrasonic vibration for SEM imaging.

Fig. 3 shows typical SEM micrographs of ZrN–Alon composites. It is seen that the ZrN particles were basically uniformly distributed in the Alon matrix, in spite of some conglomerations appeared. Since the volume would be decreased during the phase change from ZrO_2 to ZrN, the particles of fabricated ZrN would still be nano-sized. The pure Alon contained quite a number of pores which were also homogeneously dispersed as well. With increasing amount of ZrN particles the number of pores visibly decreased, which could be quantified via the Archimedes principle and quantitative image analysis.

Fig. 4 shows the open-porosity and relative density of the composites as a function of ZrN content. It is seen that the open-porosity decreased slightly with increasing amount of ZrN particles, meanwhile the relative density (i.e., the density with respect to the theoretical density) increased. The values shown in Fig. 4 were based on the theoretical densities of 3.688 g/cm^3 and 7.09 g/cm^3 for Alon and ZrN, respectively. Higher densifi-

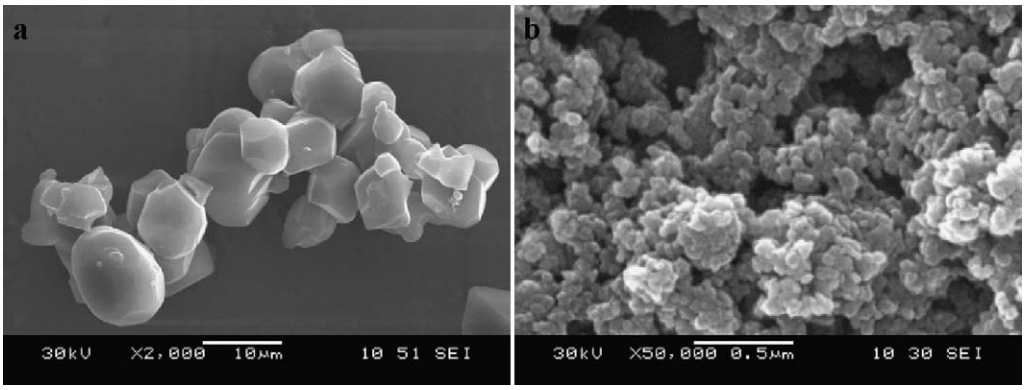

Fig. 2. SEM micrographs of raw powders for (a) the prepared Alon powders and (b) the nano-sized ZrO_2 powders.

cation was achieved for ZrN–Alon composites, indicating that the amount of ZrN particles played an important role in enhancing the relative density. While a relative density of 97.6% for pure Alon was obtained, a relative density of 99.5% in the composites with the addition ZrN particles was achieved using the present hot-press sintering process. When the amount of ZrN particles reached up to 2.7%, the relative density of the composites increased obviously. A further addition of ZrN particles from 2.7% to 4.1% only gave rise to a slight increase. As seen from Fig. 4, the open-porosity decreased with increasing ZrN particles, corresponding well to the change of the relative density.

Fig. 5 shows the variation of the porosity in the Alon matrix composites with ZrN particles, determined using a quantitative image analysis system. It is seen that the porosity decreased with increasing amount of ZrN particles, which was in good agreement with the relative density measured via the Archimedes principle (Fig. 4). It is clear that the nano-sized ZrN particles played a key role in the densification of ZrN–Alon composites. Details will be presented in Section 4.

3.3. Mechanical properties

Fig. 6 shows the change of microhardness with the amount of ZrN particles, and Fig. 7 demonstrates the dependence of Young's modulus on the content of ZrN particles and porosity at room temperature. The microhardness is a valuable mechanical property for ceramics, which is often utilized when an abrasive or grinding action is required. It is seen from Figs. 6 and 7(a) that both the microhardness and Young's modulus of ZrN–Alon

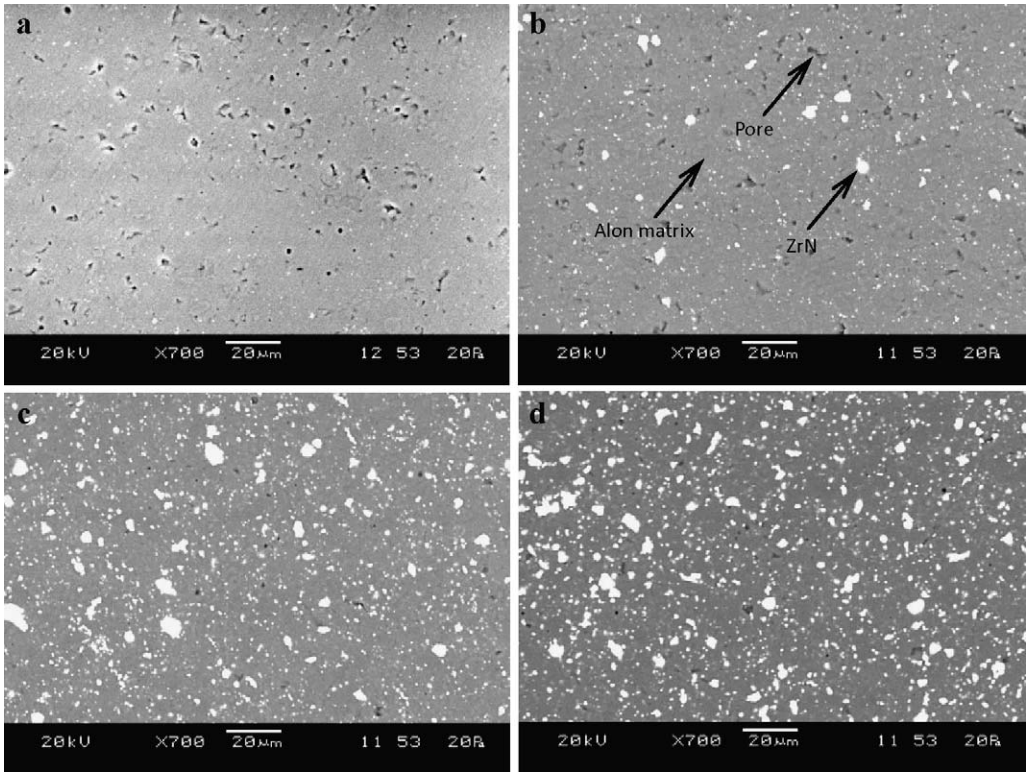

Fig. 3. SEM micrographs of the synthesized ZrN–Alon composites: (a) pure Alon, (b) 1.4% ZrN, (c) 2.7% ZrN and (d) 4.1% ZrN.

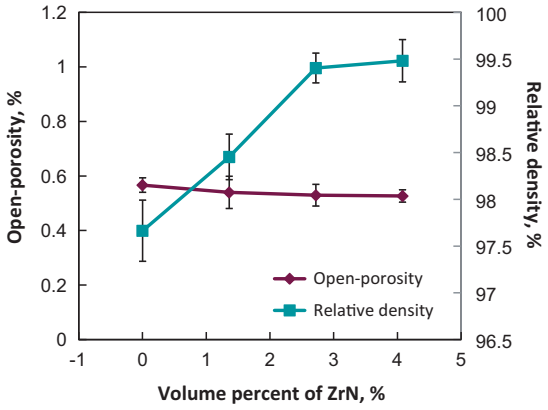

Fig. 4. Variation of the open-porosity and relative density measured via the Archimedes principle with the amount of ZrN particles in the ZrN–Alon composites.

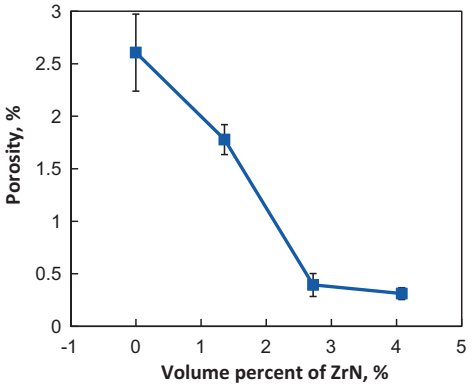

Fig. 5. Variation of the porosity, determined via the image analysis of SEM images, with the amount of ZrN particles in the ZrN–Alon composites.

composites increased with increasing content of ZrN particles. A detailed explanation on the dependence of microhardness on the amount of ZrN particles and Young's modulus on the amount of ZrN particles and porosity will be given in Section 4.

Fig. 8 shows the flexural strength and fracture toughness as a function of ZrN amount. It is seen that both the flexural strength and fracture toughness markedly increased with increasing amount of ZrN particles up to about 2.7%. This would be partly

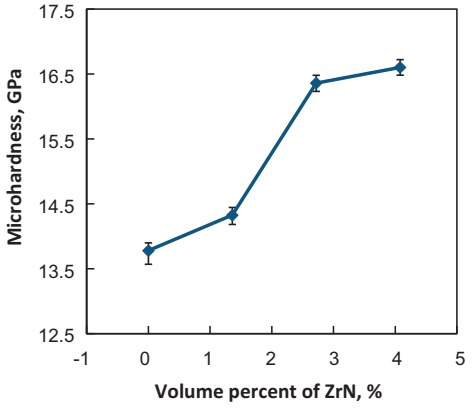

Fig. 6. Microhardness as a function of the amount of ZrN particles in the ZrN–Alon composites.

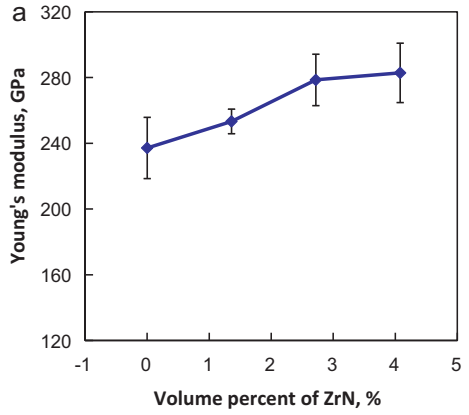

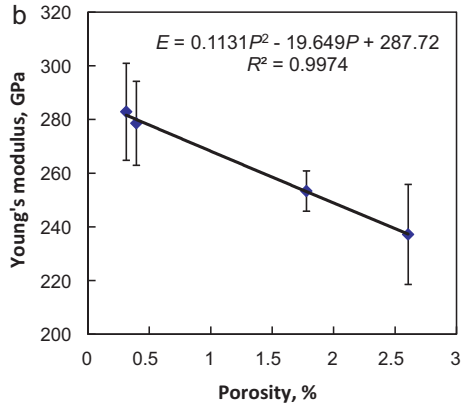

Fig. 7. Young's modulus as a function of (a) the amount of ZrN particles and (b) the porosity in the ZrN–Alon composites.

attributed to the increase in the relative density (Fig. 4) and the decrease in the porosity (Fig. 5). It is seen that the value of flexural strength obtained in the present pure Alon was equal to that (300.1 MPa) reported in[31] within the experimental scatter, but the value of fracture toughness in the pure Alon (1.54 MPa $m^{1/2}$) was somewhat lower than that (2.0 MPa $m^{1/2}$) given in.[31] This would partly be related to the use of the indentation technique, since the toughness values evaluated from the indentation-induced crack size measurements were reported to be consistently lower than those determined by conventional measurements typically by about 30%.[32] The flexural strength and the fracture toughness of the composite with 2.7% ZrN par-

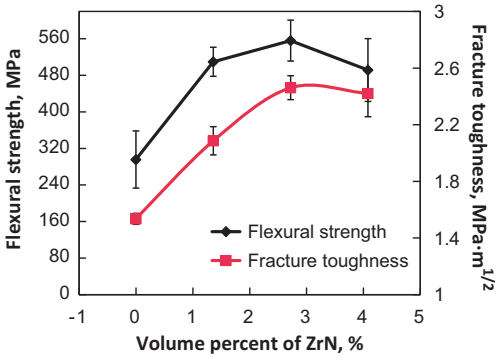

Fig. 8. Flexural strength and fracture toughness as a function of the amount of ZrN particles in the ZrN–Alon composites.

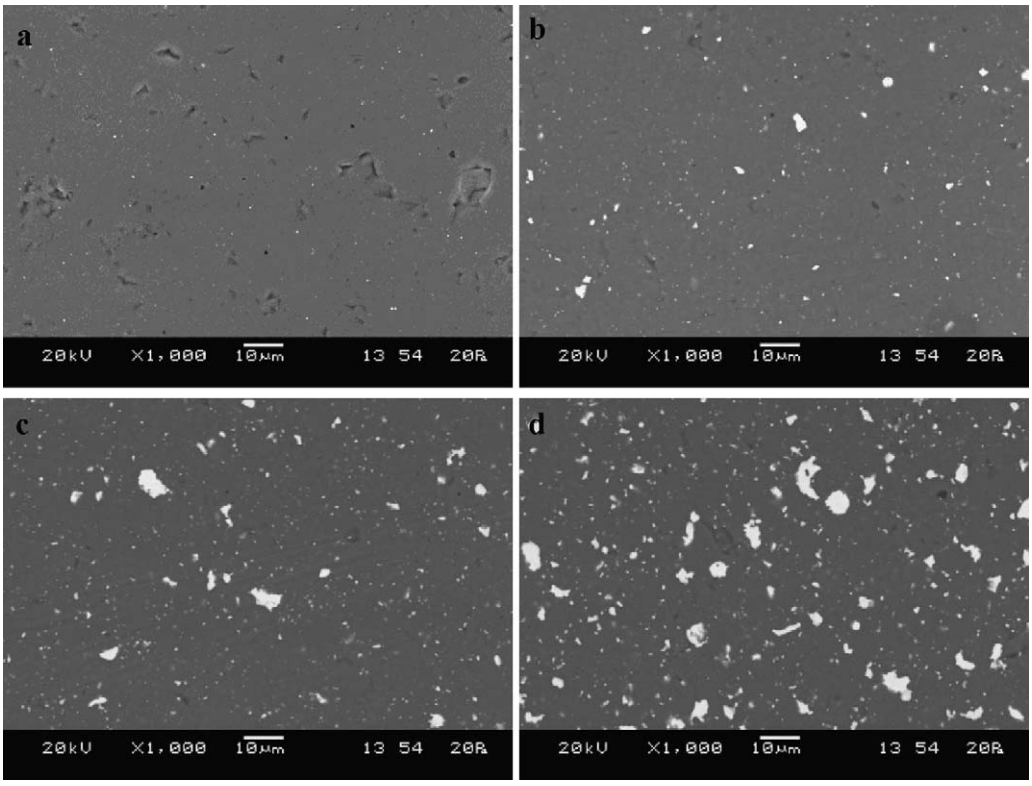

Fig. 9. Backscattered electron images of ZrN–Alon composites: (a) pure Alon, (b) 1.4% ZrN, (c) 2.7% ZrN and (d) 4.1% ZrN.

ticles reached the highest value of 555 MPa and 2.5 MPa $m^{1/2}$, respectively. However, when the concentration of ZrN particles increased to 4.1% both flexural strength and fracture toughness exhibited a slight decrease, although pure zirconium nitride itself exhibited higher fracture toughness. This might be associated with more obvious agglomerates in the 4.1% ZrN composite as seen from the backscattered electron images in Fig. 9. As reported in,[33] zirconium nitride exhibited fairly low flexural strength. The improvement in the mechanical properties achieved by the incorporation of a dispersion of ZrN particles in crystalline ceramic matrices depended on the volume fraction of zirconium nitride. This indeed reflected a reduction of porosity with increasing amount of ZrN particles, thus giving rise to an increase of the flexural strength and fracture toughness by 88% and 60% in comparison to the pure Alon, respectively. Other underlying toughening mechanisms will be discussed later.

Fig. 10 shows typical SEM micrographs of fracture surfaces of sintered pure Alon and composites with 1.4%, 2.7% and 4.1% ZrN particles after TPB tests. It is seen that the fracture surface of pure Alon basically exhibited an intergranular fracture mode in conjunction with some cleavage fracture features – a typical brittle fracture surface like most common ceramics. With increasing ZrN particles, more transgranular cracking together with some ridge-like features was observed, which was similar to some other ceramic composite materials.[34] Fig. 10 also gives clear evidence that the presence of nano-sized ZrN particles effectively restricted the growth of grains during sintering at 1850 °C, leading to an obvious refined grain size. Similar result was also reported in hot-pressed $MoSi_2$-matrix composites reinforced with SiC and ZrO_2 particles.[35] This was attributed to the pinning effect of ZrN nano-particles located at Alon grain boundaries, as seen better from the backscattered electron images shown in Fig. 11. A detailed explanation will be given in the next section.

4. Discussion

In the present study, a new type of nano-sized ZrN particulate reinforced Alon composites with better mechanical properties and fracture resistance has been successfully fabricated. Due to the presence of nano-sized ZrN particles, both flexural strength and fracture toughness were remarkably improved. In this section the role of the ZrN nano-particles in improving mechanical properties, especially the salient strengthening and toughening mechanisms, will be discussed.

4.1. Density, microhardness and Young's modulus

As presented in Figs. 4 and 5, the porosity decreased and the relative density increased with increasing amount of ZrN particles. This indicated that the presence of ZrN in the Alon matrix played a significant role. Since the average size of ZrN particles was very small, i.e., in the nanometer scale (Fig. 2(b)), it was easy for the miniature particles to get into grain boundaries or triple junctions of micro-scale Alon particles (Fig. 2(a)). The ZrN particles pinned the Alon grain boundaries so that grain boundary movement was hampered and pores can be removed

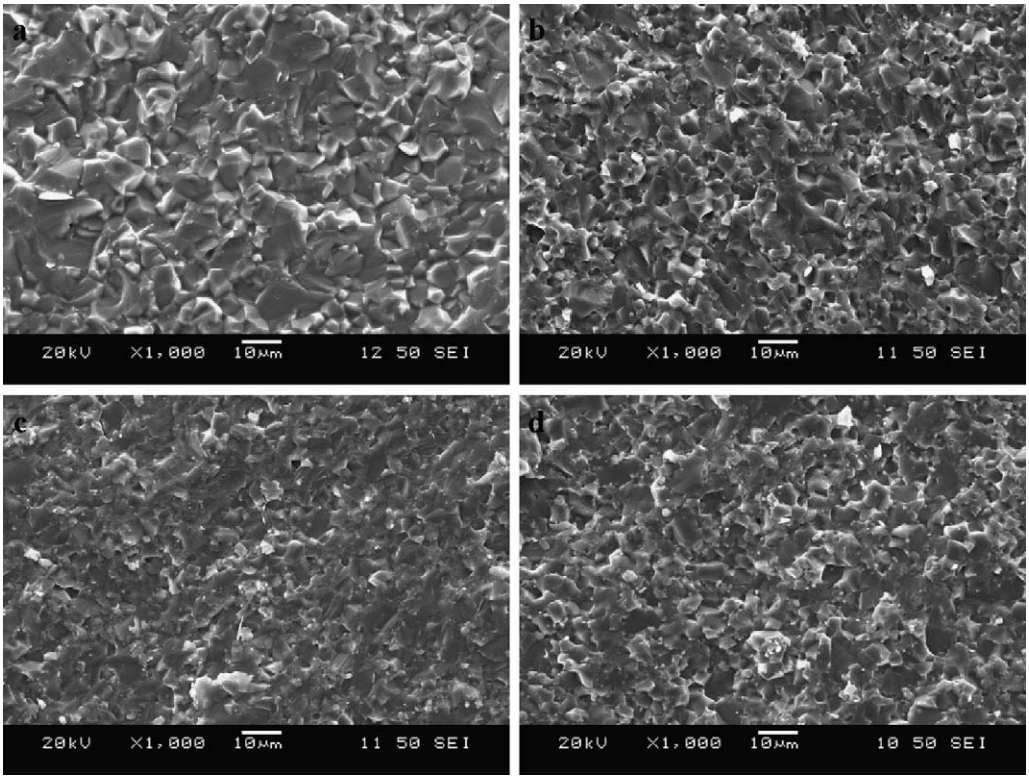

Fig. 10. SEM images of fracture surfaces after three point bending tests: (a) pure Alon, (b) 1.4% ZrN, (c) 2.7% ZrN and (d) 4.1% ZrN.

from the Alon grains and ZrN particles remained mostly between the Alon grains, as shown in Fig. 11. Similar observations in alumina–zirconia ceramics were reported as well.[36]

It can be seen from Fig. 6 that the microhardness of ZrN–Alon composites increased with increasing content of ZrN particles. This was related to three potential reasons: first, the hardness of pure ZrN particles is higher than that of pure Alon. Based on the rule of mixtures,[26] the hardness of ZrN–Alon composites should increase with increasing content of the ZrN particles. Second, the porosity had a significant effect on the hardness. It has been observed that the hardness of ceramics can be estimated using the following empirical expression,[37]

$$H = H_o \exp(-cP) \quad (4)$$

where H_o is the hardness of the fully dense ceramics, P is the volume fraction of the porosity, and c is an empirical constant. According to Eq. (4), the lower the porosity or the higher the density, the higher the hardness of ceramics. Third, the ZrN particles would impede grain growth during the high-temperature sintering. When the matrix grain size was larger than a critical grain size (about 10–50 nm depending on materials), the hardness would increase with decreasing grain size as reported in,[38,39] where the Hall–Petch relation holds true.

It has been reported that porosity was a major factor governing Young's modulus of porous bodies.[40] For some ceramic materials the magnitude of Young's modulus E (GPa) decreased with increasing porosity P (%) according to the following empir-

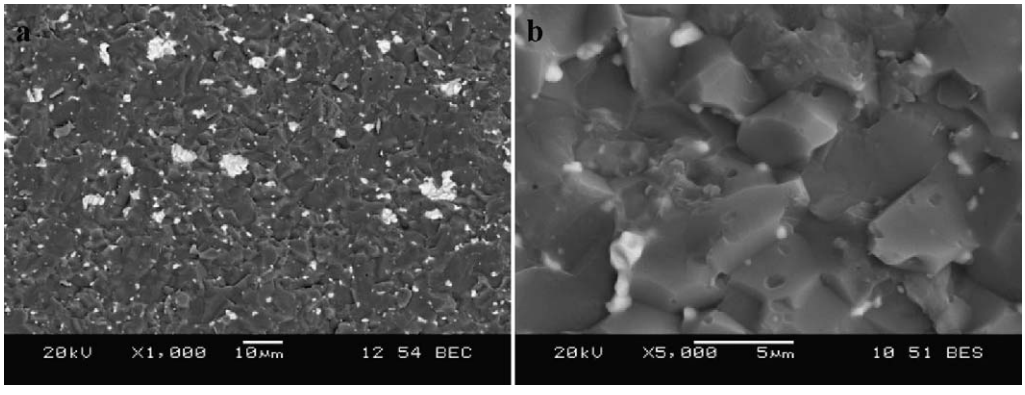

Fig. 11. Backscattered electron images of fracture surfaces with 4.1% ZrN–Alon composites, where the ZrN particles are mostly located at Alon grain boundaries, taken at (a) a lower magnification and (b) a higher magnification.

ical equation,[26]

$$E = E_o(1 - \alpha P + \beta P^2), \quad (5)$$

where E_o is the Young's modulus of nonporous materials, α and β are two positive constants. As seen in Fig. 7(b), the results obtained in the present study followed Eq. (5) well with E_o being 288 GPa, α and β being 0.068 and 0.0004, respectively. The influence of porosity on the Young's modulus in the ZrN–Alon composites was similar to that in aluminium oxide material.[26] From Eq. (5) it is clear that the higher the amount of porosity, the lower the Young's modulus. In other words, Young's modulus increased with increasing density. Therefore, the nano-sized ZrN particles led to an increased value of Young's modulus in the ZrN–Alon composites with increasing amount of ZrN particles or decreasing porosity, as shown in Fig. 7(a) and (b).

4.2. Strengthening and toughening mechanisms

The flexural strength and fracture toughness of ceramic materials are important mechanical properties and crucial for their applications. As shown in Fig. 8, the presence of ZrN particles in the present study significantly improved the mechanical properties of Alon ceramic. Some possible mechanisms for the improvement are discussed as follows.

First, the fracture toughness of a material is dependent on its microstructure.[41] In the present study, the nano-sized ZrN particles were homogeneously distributed in the Alon matrix (Fig. 2). These particles could create mechanically interlocked interfaces between ZrN particles and Alon matrix, thus increasing the resistance of crack growth. Besides, the influence of ZrN on the microstructure was also reflected by its obvious role to inhibit the grain growth, as observed in Fig. 10. As mentioned earlier, this was mainly attributed to the pinning effect of small ZrN particles located at grain boundaries or triple junctions of Alon (Fig. 11). The flexural strength would increase with the refined grains.[42] The strong pinning effect at the grain boundaries of alumina–zirconia ceramics was also reported after sintering for the long isothermal period.[36]

Second, different microstructures could steer various mechanisms, such as, crack bridging and crack deflection which could enhance the flexural strength and fracture toughness.[14,18,34,43] Fig. 12 shows some typical examples on the crack bridging, crack branching and crack deflection observed in the ZrN–Alon composites after Vickers indentation tests. The crack propagation path in the pure Alon was fairly straight (Fig. 12(a)), which was typical for brittle materials. When the ZrN particles were present in the Alon matrix, the crack path became tortuous (Fig. 12(b)). As seen from Fig. 12(c)–(e), some ZrN particles cracked when the Alon matrix crack reached them, but they made the crack redirected or deflected as indicated by the arrows. Meanwhile, these ZrN particles also played a bridging role; this might be better seen from Fig. 12(e). Crack branching could be seen from both Fig. 12(e) and (f), and crack deflection could be clearly seen in Fig. 12(f) as well. Consequently, the major toughening mechanisms in the ZrN–Alon composites were crack bridging, branching and deflection. The observed crack bridging, branching and deflection would consume more energy and lead to an increase in the resistance to crack propagation, thus increasing the flexural strength and fracture toughness as shown in Fig. 8. In addition, the combination of the fracture mode exhibiting both intergranular and transgranular cracking (Fig. 10) with the ZrN particles positioned at the grain boundaries (Fig. 11) can alter the path of a crack impinging on a boundary enough to change both the fracture behaviour and the measured fracture toughness, as also reported in.[44,45] Therefore, by incorporating ZrN particles into the Alon matrix the bending strength and fracture toughness of the composites effectively increased.

Lastly, as mentioned before, porosity in the sintered materials has an important influence on Young's modulus and microhardness. It should also have an effect on the fracture toughness and flexural strength. Indeed a similar dependence of these characteristics on the porosity has been reported by Choi et al.[46] The porosity was detrimental to the flexural strength for two reasons: (i) pores reduced the cross-sectional areas across which a load was applied, and (ii) they also acted as stress concentrators, e.g., for an isolated spherical pore, an applied tensile stress would be amplified by a factor of 2. An empirical relationship between the flexural strength (σ_{FS}) and porosity (P) could be expressed as[26]:

$$\sigma_{FS} = \sigma_o \exp(-nP), \quad (6)$$

where σ_o and n are two constants determined experimentally. It follows that the flexural strength decreased exponentially with porosity. In the present study the dispersion of nano-sized ZrN particles into the micro-sized Alon matrix, as seen in Fig. 3 and represented by the enhanced density and lowered porosity (Figs. 4 and 5), was another factor for effectively improving the flexural strength shown in Fig. 8. The similar change trend of the fracture strength and fracture toughness with increasing amount of ZrN particles might be understood from the following relationship,[34,47]

$$\sigma_{FS} = \left(\frac{K_c}{2}\right) \cdot \left(\frac{\pi}{a}\right)^{1/2}, \quad (7)$$

where σ_{FS} is the flexural strength, a is the flaw size, and K_c is the fracture toughness. It is seen that the fracture strength increased with increasing fracture toughness. However, when the amount of ZrN particles increased from 2.7% to 4.1%, both flexural strength and fracture toughness decreased. This was mainly due to the obvious agglomerates of ZrN particles as seen in Fig. 9(d). This investigation thus shows that the presence of about 2.7% ZrN particles gives rise to the optimal flexural strength and fracture toughness under the present hot-press sintering condition. More studies are needed to reduce the agglomerates of ZrN nano-particles with a volume percent of 4.1% or higher so as to further enhance the mechanical properties and fracture toughness of the ZrN nano-particulate reinforced Alon composites.

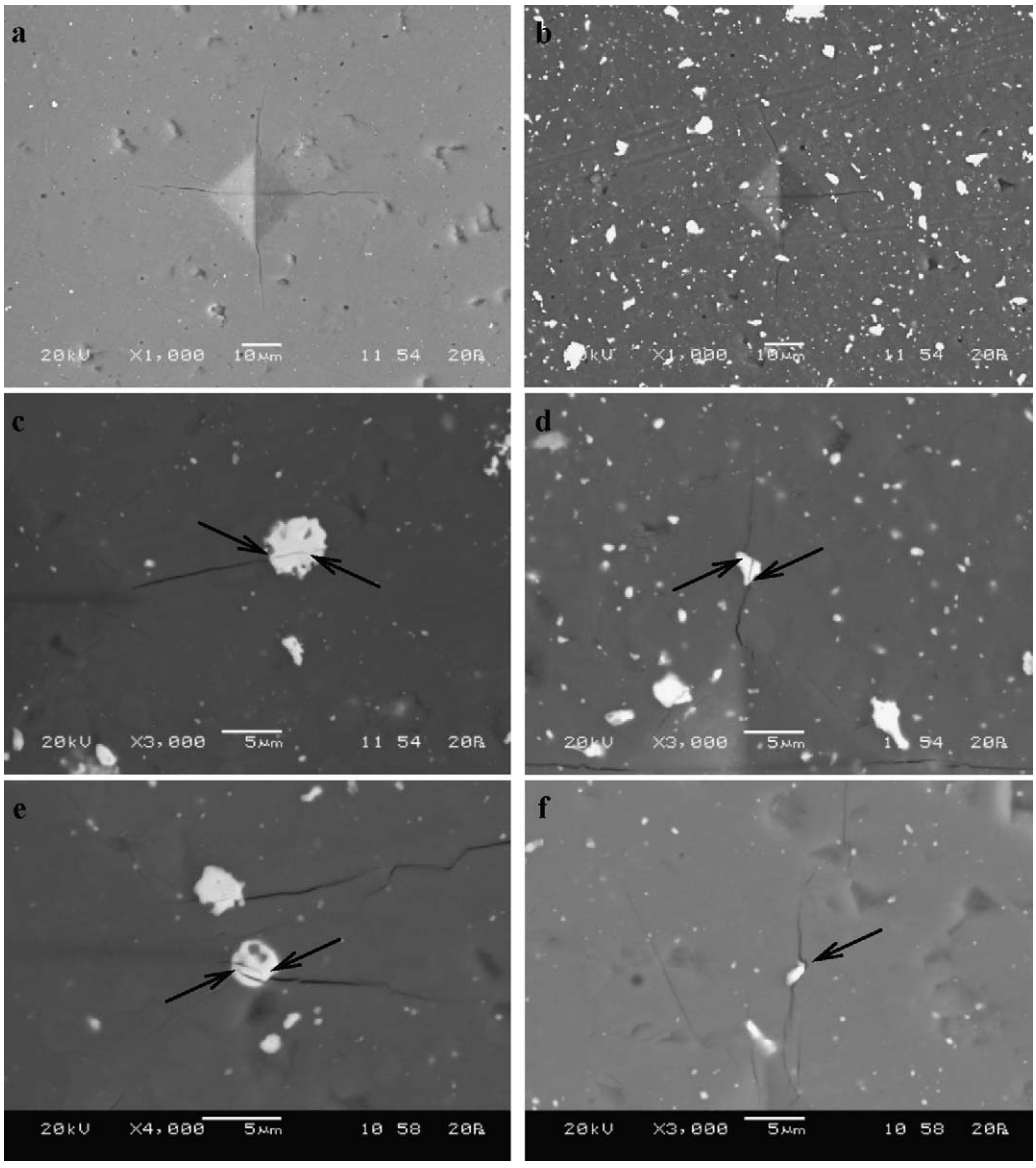

Fig. 12. SEM images of indentation crack propagation in (a) pure Alon and (b–f) ZrN–Alon composites.

5. Conclusions

In the present study a new type of aluminium oxynitride (Alon) based composites with effectively improved mechanical properties and fracture resistance has been achieved by zirconium nitride (ZrN) phase arising from adding nano-sized zirconia (ZrO_2) particles via hot-press sintering. It was observed that the presence of ZrN nano-particles led to pinning effect of ZrN nano-particles positioned at grain boundaries or triple junctions of micro-scale Alon particles, and constrained the growth of Alon grains during sintering and thus reduced the grain size in the nano-particulate reinforced composites. With increasing amount of ZrN nano-particles up to 2.7%, the relative density, hardness, Young's modulus, flexural strength, and fracture toughness all increased. When the amount of ZrN nano-particles surpassed 2.7%, while the density, hardness and Young's modulus continued to increase moderately, the flexural strength and fracture toughness displayed a slight decrease due to the occurrence of agglomerates of ZrN nano-particles. A variety of toughening mechanisms in the ZrN nano-particulate reinforced Alon composites such as microcrack toughening, crack deflection, crack bridging and crack branching were observed, hence increasing effectively the crack propagation resistance and resulting in a significant improvement in the flexural strength and fracture toughness of the composites.

Acknowledgments

The authors would like to thank the financial support of Natural Sciences and Engineering Research Council of Canada (NSERC) and the National Natural Science Foundation of China (NSFC grant number 50672060) in the form of international research collaboration. D.L. Chen is also grateful for the financial support by the Premier's Research Excellence Award (PREA), Canada Foundation for Innovation (CFI), and Ryerson Research Chair (RRC) program. The authors would also

like to thank Professor X. D. Sun (Northeastern University) for the helpful discussion and suggestion, and Q. Li, A. Machin, J. Amankrah and R. Churaman (Ryerson University), X.Y. Wang and H.M. Kan (Shenyang University) for their assistance in the experiments. X.J. Zhao, as an international exchange Ph.D. student, also gratefully acknowledges the financial support provided by China Scholarship Council.

References

1. Corbin ND. Aluminum oxynitride spinel: a review. *J Eur Ceram Soc* 1989;**5**:143–54.
2. Yamaguchi G, Yanagida H. Study on the reductive spinel—a new spinel formula AlN–Al_2O_3 instead of the previous one Al_3O_4. *Bull Chem Soc Jpn* 1959;**32**:1264–5.
3. Willems HX, Hendrix MMRM, Metselaar R, de With G. Thermodynamics of Alon. I: Stability at lower temperatures. *J Eur Ceram Soc* 1992;**10**:327–37.
4. Wang XD, Li WC, Seetharaman S. Thermodynamic study and synthesis of γ-aluminum oxynitride. *Scand J Metall* 2002;**31**:1–6.
5. McCauley JW, Patel P, Chen MW, Gilde G, Strassburger E, Paliwal B, Ramesh KT, Dandekar DP. AlON: a brief history of its emergence and evolution. *J Eur Ceram Soc* 2009;**29**:223–36.
6. Wang XD, Wang FM, Li WC. Synthesis, microstructures and properties of γ-aluminum oxynitride. *Mater Sci Eng A* 2003;**342**:245–50.
7. Zheng J, Forslund B. Carbothermal synthesis of aluminium oxynitride (AlON) powder: influence of starting materials and synthesis parameters. *J Eur Ceram Soc* 1995;**15**:1087–100.
8. McCauley JW, Corbin ND. Phase relations and reaction sintering of transparent cubic aluminum oxynitride spinel (AlON). *J Am Ceram Soc* 1979;**62**:476–9.
9. Wu D, Zhang Z, Fu W, Fan X, Guo H. Structure, electrical and chemical properties of zirconium nitride films deposited by dc reactive magnetron sputtering. *Appl Phys A* 1997;**64**:593–5.
10. Adachi J, Kurosaki K, Uno M, Yamanaka S. Thermal and electrical properties of zirconium nitride. *J Alloys Compd* 2005;**399**:242–4.
11. Fu B, Gao L. Synthesis of nanocrystalline zirconium nitride powders by reduction–nitridation of zirconium oxide. *J Am Ceram Soc* 2004;**87**:696–8.
12. Li XY, Li GB, Wang FJ, Ma TC, Yang DZ. Investigation on properties of ceramic coatings of ZrN. *Vacuum* 1992;**43**:653–6.
13. Schwarz K, Williams AR, Cuomo JJ, Harper JHE, Hentzell HTG. Zirconium nitride—a new material for Josephson junctions. *Phys Rev B* 1985;**32**:8312–6.
14. Montazerian M, Alizadeh P, Yekta BE. Pressureless sintering and mechanical properties of mica glass–ceramic/Y-PSZ composite. *J Eur Ceram Soc* 2008;**28**:2687–92.
15. Baun WL. Phase transformation at high temperatures in hafnia and zirconia. *Science* 1963;**140**:1330–1.
16. Evans PE, Wildsmith G. Evidence of phase changes in zirconia from thermal etching. *Nature* 1961;**189**:569–70.
17. Bocanegra-Bernal MH, de la Torre SD. Phase transition in zirconium dioxide and related materials for high performance engineering ceramics. *J Mater Sci* 2002;**37**:4947–71.
18. Hannink RHJ, Kelly PM, Muddle BC. Transformation toughening in zirconia-containing ceramics. *J Am Ceram Soc* 2000;**83**:461–87.
19. Weiss J, Gauckler LJ, Tien TY. The system Si_3N_4–SiO_2–ZrN–ZrO_2. *J Am Ceram Soc* 1979;**62**:632–4.
20. Goeuriot P, Goeuriot-Launay D, Thebenot F. Oxidation of Al_2O_3–γAlON ceramic composite. *J Mater Sci* 1990;**25**:654–60.
21. Akihiro S, Hideo I, Masanori U. AlON and its ceramics. *J Ceram Soc Jpn* 1992;**100**:504–8.
22. Zhang ZT, Li WC, Bater SY. Manufacture and properties of AlON–TiN particulate composites. *Mater Des* 2005;**26**:363–8.
23. Yamashita H, Yamaguchi A. Preparation and properties of AlON–SiAlON composites. *J Ceram Soc Jpn* 2001;**109**:434–9.
24. Khan IA, Hassan M, Hussain T, Ahmad R, Zakaullah M, Rawat RS. Synthesis of nano-crystalline zirconium aluminium oxynitride (ZrAlON) composite by dense plasma focus device. *Appl Surf Sci* 2009;**255**:6132–40.
25. Ahn ES, Gleason NJ, Ying JY. The effect of zirconia reinforcing agents on the microstructure and mechanical properties of hydroxyapatite-based nanocomposites. *J Am Ceram Soc* 2005;**88**:3374–9.
26. Callister WD. In: Hayton J, editor. *Materials science and engineering: an introduction*. New York: John Wiley & Sons, Inc.; 2007. p. 412–606.
27. Dowling NE. In: Stark H, editor. *Mechanical behavior of materials: engineering methods for deformation, fracture, and fatigue*. Upper Saddle River, NJ: Pearson Education, Inc.; 2007. p. 152–4.
28. Kruzic JJ, Ritchie RO. Determining the toughness of ceramics from Vickers indentations using the crack-opening displacements: an experimental study. *J Am Ceram Soc* 2003;**86**:1433–6.
29. Anstis GR, Chantikul P, Lawn BR, Marshall DB. A critical evaluation of indentation techniques for measuring fracture toughness: I. Direct crack measurements. *J Am Ceram Soc* 1981;**64**:533–8.
30. Qi JQ, Zhou JC, Pang W, He JF, Su YY, Liao ZJ, Wu DX, Lu TC. Study on the preparation of AlON powder by solid state reaction method. *Rare Metal Mater Eng* 2007;**36**:88–91.
31. Quinn GD, Corbin ND, McCauley JW. Thermomechanical properties of aluminium oxynitride spinel. *Am Ceram Soc Bull* 1984;**63**:723–30.
32. Gatto A. Critical evaluation of indentation fracture toughness measurements with Vickers indenter on ceramic matrix composites tools. *J Mater Process Technol* 2006;**174**:67–73.
33. Alexandre N, Desmaison-Brut M. Mechanical properties of hot isostatically pressed zirconium nitride materials. *J Mater Sci* 1993;**28**:2385–90.
34. Chang Q, Chen DL, Ru HQ, Yue XY, Yu L, Zhang CP. Toughening mechanism in iron-containing hydroxyapatite/titanium composites. *Biomaterials* 2010;**31**:1493–501.
35. Ma Q, Yang YQ, Kang MK, Xue QJ. Microstructures and mechanical properties of hot-pressed $MoSi_2$-matrix composites reinforced with SiC and ZrO_2 particles. *Compos Sci Technol* 2001;**61**:963–9.
36. Wang CJ, Huang CY, Wu YC. Two-step sintering of fine alumina–zirconia ceramics. *Ceram Int* 2009;**35**:1467–72.
37. Chaim R, Hefetz M. Effect of grain size on elastic modulus and hardness of nanocrystalline ZrO_2–3 wt% Y_2O_3 ceramic. *J Mater Sci* 2004;**39**:3057–61.
38. Deng XY, Wang XH, Gui ZL, Li LT. Grain-size effects on the hardness of nanograin $BaTiO_3$ ceramics. *J Electroceram* 2008;**21**:238–41.
39. Hardness-grain-size relations in ceramics. *J Am Ceram Soc* 1994;**77**:2539–53.
40. Feldman RF. Factors affecting Young's modulus-porosity relation of hydrated Portland cement compacts. *Cem Concr Res* 1972;**2**:375–86.
41. Hahn GT. Influence of microstructure on brittle fracture toughness. *Metall Trans A* 1984;**15**:947–59.
42. Oh ST, Sando M, Sekino T, Niihara K. Processing and properties of copper dispersed alumina matrix nanocomposites. *Nanostruct Mater* 1998;**10**:267–72.
43. Dauskardt RH, Yu W, Ritchie RO. Fatigue propagation in transformation-toughened zirconia ceramic. *J Am Ceram Soc* 1987;**70**:C.248–52.
44. Kueck AM, Ramasse QM, Jonghe LC, de Ritchie RO. Atomic-scale imaging and the fracture toughness of silicon carbide ceramics. *Acta Mater* 2010;**58**:2999–3005.
45. Sun XD, Li JG, Guo SW, Xiu ZM. Intragranular particle residual stress strengthening of Al_2O_3–SiC nanocomposites. *J Am Ceram Soc* 2005;**88**:1536–43.
46. Choi SR, Sanders WA, Salem JA, Tikare V. Young's modulus, strength and fracture toughness as a function of density of in situ toughened silicon nitride with 4 wt% Scandia. *J Mater Sci Lett* 1995;**14**:276–8.
47. Kruzic JJ, Satet RL, Hoffmann MJ, Cannon RM, Ritchie RO. The utility of *R*-curves for understanding fracture toughness-strength relations in bridging ceramics. *J Am Ceram Soc* 2008;**91**:1986–94.